Larhyss Journal, ISSN 1112-3680, n°56, Dec 2023, pp. 235-265

AREAL PRECIPITATION AND DEPTH-AREA DURATION CURVES FOR REGIONS IN TRINIDAD USING A TRIANGULATED GRID

BALKISSOON S.S[1], GUNAKALA S.R.[2], AZAMATHULLA H.M.[2]*

[1] Atmospheric Science Program, University of Missouri, USA
[2] Department of Mathematics and Statistics, University of the West Indies, St. Augustine Campus, Trinidad and Tobago

(*) sreedhara.rao@sta.uwi.edu

Research Article – Available at http://larhyss.net/ojs/index.php/larhyss/index
Received September 2, 2023, Received in revised form December 3, 2023, Accepted December 5, 2023

ABSTRACT

A triangulated grid was used to estimate the areal precipitation for regions in Trinidad. The rain gauge stations, from three hydrometric units, served as nodal points. Three parameters, nodal rainfall, its x and y co-ordinates, were used to determine the areal precipitation through linear interpolation. Thereafter, the total elemental volume of rainfall and the elemental average rainfall precipitation were determined. To estimate the areal precipitation of the grid for each month, a decadal (2006-2015) average of the monthly rainfall values was calculated. The largest rainfall month was November and the lowest areal precipitation occurred in March with approximately 78mm. The smaller irregular shaped elements in the mountainous regions had the most differences in areal precipitation than the other elements in the grid. Optimization of the grid was done by the reconfiguration and redistribution of the nodes. This adjusted grid resulted in more similarity in rainfall patterns for both seasons, dry and rainy. The Depth-Area Duration Curves (DAD), for each month and for each season, show the changes of the average precipitation depth with area span by the grid. Temporally, the areal precipitation were oscillating for both seasons as the years progressed from 2006-2015. It should be noted though that, as the years progressed, the amplitude of the oscillations decreased in the rainy season.

Keywords: Triangulated Grid, Areal Precipitation, Depth-Area Duration Curves (DAD)

INTRODUCTION

Precipitation measurement at a single point often does not give an accurate representation of the volume of rainfall that is falling over a particular catchment area (NOAA 2016; Task Committee on Hydrology Handbook 1996). These areal estimates of precipitation is required for hydrological analysis and modelling (NOAA, 2016; Atkin, 1971). One such model is the river forecasting model used by the National Weather Service (NWS) in which the river stage forecast is produced from the calculation of stream flow given by the runoff of sub-divided catchment areas or runoff zones (NOAA, 2016).

There are methods that are used to convert a network of precipitation measurements to an aerial estimation of precipitation. According to Dorf (2004), the mean areal precipitation can be determined by the Isohyetal Method, Theissen Polygons, Modified Polygon Method, Trend Surface Analysis, Double Fourier Series, Analysis of Variance, Two Axis Method, Kriging, Reciprocal Distance Square Method, Triangular Area Weighted Method, Individual Area-Altitude Weighted Mean, Group Area Aspect Weighted Mean, Unweighted Mean and the method using Finite Elements. Some of these methods can be seen below in Fig. 1. However, in this study, the method of triangulation is used.

Integral, differential and algebraic equations are used to describe natural phenomenon such as the simulations of weather in order to understand the mechanics of it and thus be able to make forecasts (Reddy, 1993). Since due to the complexity of the systems under various physical conditions, the equations in many cases cannot be solved analytically but rather numerically. The estimated solution of the region is given by (1)

$$u = \sum_j c_j \Phi_j \tag{1}$$

where cj are undetermined coefficients which satisfies the integral equation hence the differential equation and Φj are approximation functions.

In this numerical method of triangulation, u is a linear combination of uj and φj where uj are the values of u at the nodal points and Φj are interpolation functions which are algebraic polynomials. According to Reddy (1993), it has steps which firstly involves the discretization of the domain into a mesh of finite elements be it triangular, quadrilateral or both elements; these are representative of the geometry and the solution of the problem. Thereafter, on an elemental scale, the estimate values of the field variable is determined as a linear combination of the nodal values and the finite element approximation functions or interpolation functions. Finally, the third step is the derivation of the algebraic equations which relates the elemental solution values at the nodes and the assemblage of all the elements which comprises of the domain to obtain a solution for the entire region. There are advantages of using this method. It permits the discretization of irregular domains into a mesh of multiple elements. This ensures the accurate geometric representation of the region which in turns results in an accurate approximation of the field variable, u. Also, since approximation of the solution is done at an elemental level; that is it is a piecewise estimation of u, discontinuous data is allowed in the approximation (Reddy 1993; Mampitiya, 2023).

Even though the arithmetic method is a simpler to determine the average rainfall than triangulation method, it does not have the ability to assign unequal weights to various locations. The discretized mesh allows the flexibility to choose the number of connections of stations thus allowing the ability to assign more weights to the more accurate rain gauge stations. The mesh determines the accuracy of the average precipitation of the domain. A linear interpolation is used to determine the precipitation distribution between stations. This is an assumption made using this methodology and thus the accuracy of the mean areal precipitation depends on the fineness of the mesh or the greater number of nodes and subsequently elements of the grid. The triangulated mesh method can facilitate changes without difficulty and significant changes. This is particularly important in this research in Trinidad as grids need to be altered when stations are deemed non-functional and new rain gauge stations are constructed. Another significant advantage of this method is the easy generation of the Depth-Area Duration Curves. The results from the mean areal precipitation can be used to generate these plots which are useful in hydrometric analysis. From the study by Akin (Atkin, 1971), it was shown that this method proved to be accurate as its DAD Curves were comparable to the Isohyetal Method using the same domain and data. The Isohyetal method is the most accurate of the three mentioned methods; Arithmetic Mean Method, Thiessen Method and Isohyetal Method, when the contouring are drawn accurately. Hence, the Triangulated Grid Method, is accurate and as such this technique is used in this study.

The domain of this study is areas within Trinidad. It is located 10° 02’ to 10° 50’ N latitude and 60° 55’ to 61° 56’ W longitude (Darsan 2013, 151-168). This island has a land area of 4826 square km (WRA, 2017). Fig. 2 depicts the topography of Trinidad (Darsan 2013, 151-168). We observe that there are three labelled areas of elevation; they are the Northern Range, the Central Range and the Trinity Hills. The elevation of the island’s ranges decreases from North to South (WRA, 2001). Trinidad has two distinct seasons; the dry season which spans from January to May and the wet season which starts in June and ends in December. The mid- Atlantic low pressure trough is an influential factor of the rainfall experienced in the dry and wet seasons with the Inter Tropical Convergence Zone (ITCZ) being the most significant low pressure zone. The maximum annual rainfall in Trinidad is cited in the North Eastern part of the Northern Range. This is as a result of the orographic effect caused by this mountainous terrain which has a maximum altitude of 940 m. The maximum mean annual rainfall for the island given from the North Eastern area of the Northern Range is 3800 mm (Srivastava, 2017).

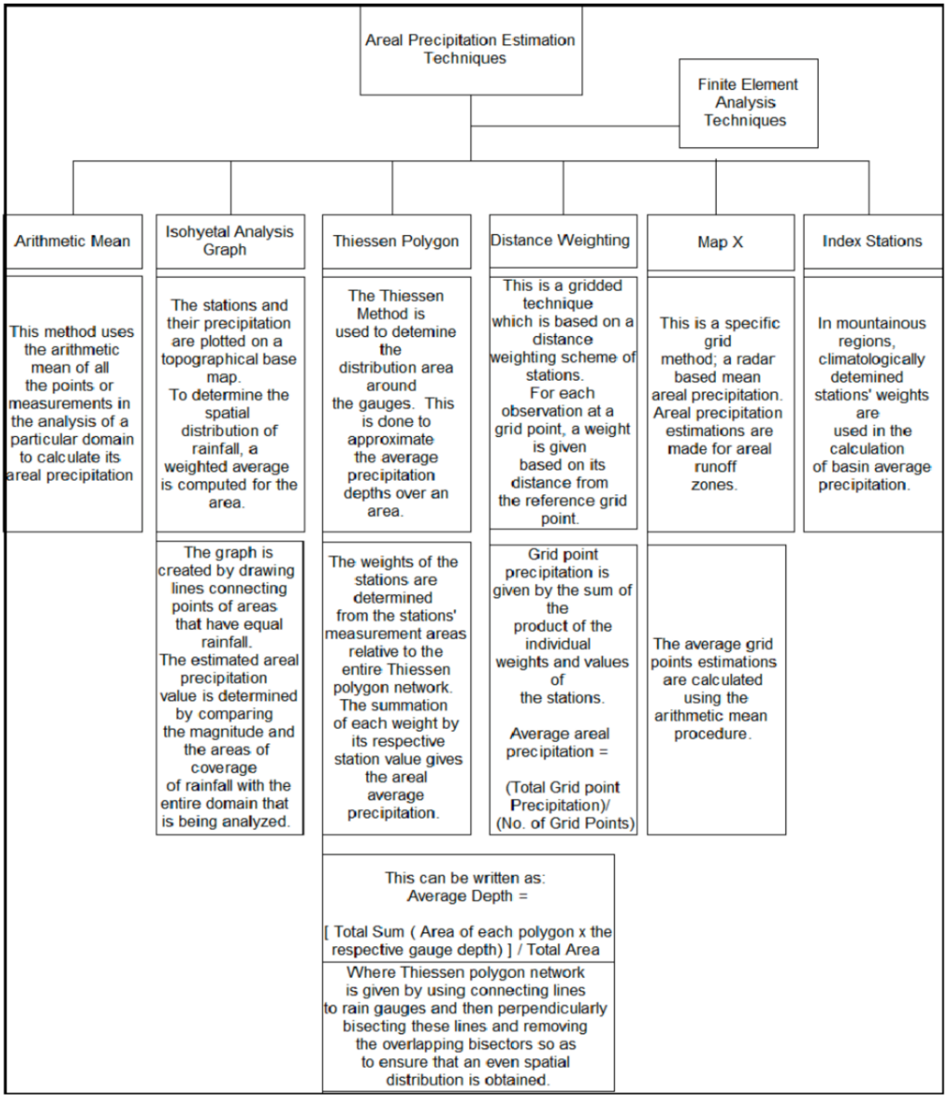

Figure 1. Methods of estimating ariel precipitation

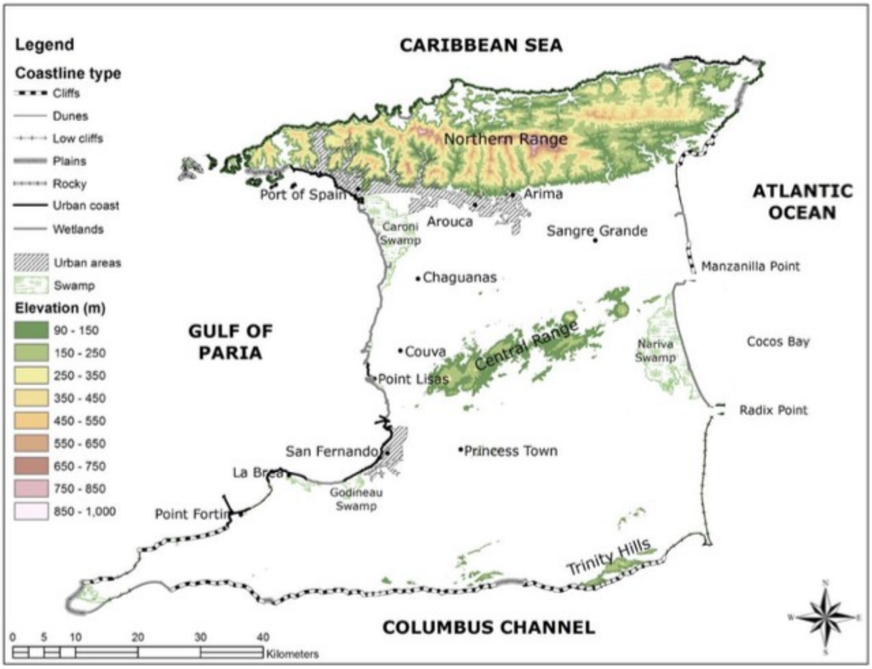

Figure 2: Topographical Map of Trinidad, *Source:* (Darson 2013)

There are three precipitation types, convective, orographic and frontal. For this study's domain, an area in the tropics, the rainfall is usually convective in nature. For this type of rainfall, rain gauges cannot accurately represent the rainfall spatial variability. Thus, a network of rain gauges is needed to determine the areal precipitation (Balkissoon 2014). According to Brakensiek et al., some of the factors that must be considered when designing a network of rain gauges are the domain size, the topography of the area of study, the type of rainfall and finally the purpose of the network (Balkissoon, 2014; Linsley et al., 1975). It is given in the World Meteorological Organization, Guide to Hydrometeorological Practices (Linsley et al., 1975) that for general purposes, for flat domains of temperate, Mediterranean and tropical zones the minimum precipitation gauge network density is 600 to 900 square km per station. For similar domains which are mountainous, the minimum density is 100 to 250 square km per station. For mountainous islands with irregular precipitation, 25 square km per station is required. In this study, the domain is approximately 1150 square km and the network of rain gauges consists of twelve nodal points for the initial grid and ten rain gauge stations for the altered grid. Daily rainfall data from the decadal period 2006 to 2015 were used in this study.

METHODOLOGY

The area is subdivided into a finite number of subdomains or elements using the point precipitation gauges as nodal points; this domain has 12 nodes and 16 elements. Table 1 gives the nodal points with their x and y co-ordinates in UTM and Decimal Dot system.

In the mesh, triangular elements are constructed by connecting the rain gauge stations together. The assemblage of these elements form the grid, see Fig. 4. Each element has three nodes each with nodal values x and y given from the station's co-ordinate as well as nodal value r given from the station's rainfall depth. This is tabulated in Table 2. The grid was altered; Elements 5, 6, 7, 8, 14 and 16 were removed and Nodal points 2 (Moka) and 4 (UWI) were removed from the grid. Nodes 2 and 4 are in close proximity to Nodes 1 and 3 respectively but Nodes 1 and 3 were stationed a further distance from the grid interior, thus these points were used as boundary points instead of Nodes 2 and 4 so as to cover more surface area. Also, Node 2 had significantly more missing data points than Node 1. The altered grid of 10 nodes and 10 elements is given by Fig. 5.

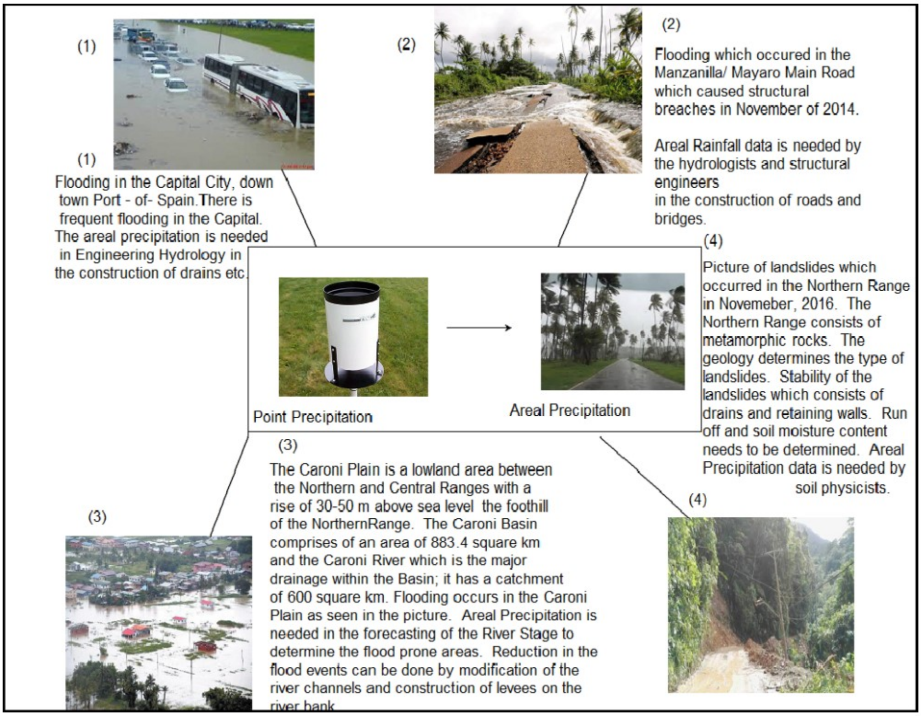

Figure 3: Importance of the determination of the areal precipitation of the domain of study

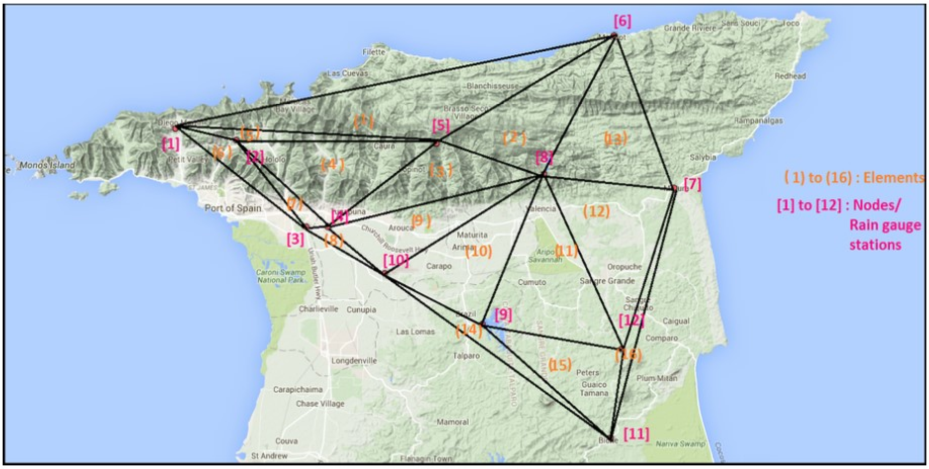

Figure 4: Map of the Mesh for Northern Trinidad

Table 1: Rain Gauge Stations and their locations

Station Name	x Co-ordinate		y Co-ordinate	
	UTM (m)	Decimal Dot (°)	UTM (m)	Decimal Dot (°)
River Estate PG	657 500	-61.55970	1 186 580	10.73077
Moka Telement	664 096	-61.49945	1 185 450	10.72027
UWI Field Station	671 770	-61.42972	1 176 270	10.63693
UWI	674 045	-61.40893	1 176 293	10.63704
Asa Wright Nature Centre	685 820	-61.30087	1 185 160	10.71663
Matelot Rest House	704 980	-61.12509	1 196 650	10.81949
Mature Police Station	711 620	-61.06530	1 180 630	10.67431
Hollis Reservoir (Quare)	697 440	-61.19482	1 182 000	10.68747
Arena Dam Pot Gauge	690 905	-61.25537	1 166 095	10.54403
Piarco	680 285	-61.35214	1 171 387	10.59239
Newlands Estate	704 820	-61.12890	1 154 125	10.43510
Grosvenor Estate	706 020	-61.11742	1 163 585	10.52055

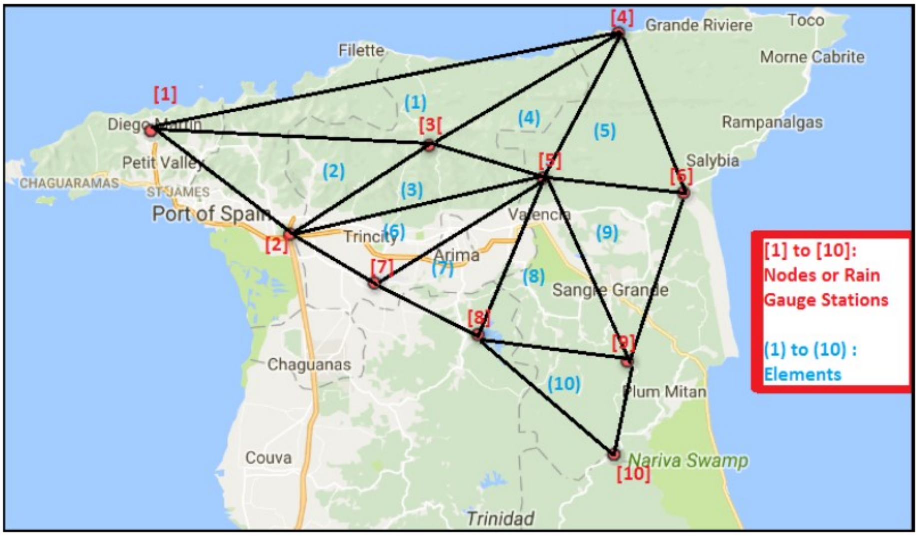

Figure 5: The Altered Grid

Fig. 5 illustrates the first element of the mesh, its nodes and the nodal point in an element can be determined by a linear interpolation using the three discrete nodal points.

Thus have, for any arbitrary point, (x_i, y_j) in the interior the n^{th} element, the rainfall value at that location is given by Equation (2) (Atkin, 1971):

$$r(x_i, y_j) = H_n(x_i, y_j) = {}_n\alpha_1 + {}_n\alpha_2 x_i + {}_n\alpha_3 y_i \tag{2}$$

where nαs are interpolation functions which contain rainfall values at a sequence of points that is, the corner gauge points Node 1r to Node 3r. It is assumed that these functions varies linearly between the gauge points thus the value of the field variable, rainfall, at any point in the sub-area of the domain can be interpolated by these function to give an approximate solution.

These functions are given by the following (Atkin 1971):

$$\begin{aligned} {}_n\alpha_1 &= \left[a_i Node\ 1r + a_j Node\ 2r + a_k Node\ 3r\right]/2A_n \\ {}_n\alpha_2 &= \left[b_i Node\ 1r + b_j Node\ 2r + b_k Node\ 3r\right]/2A_n \\ {}_n\alpha_3 &= \left[c_i Node\ 1r + c_j Node\ 2r + c_k Node\ 3r\right]/2A_n \end{aligned} \tag{3}$$

Table 2: The Nodes for each Element in the Grid and their Nodal Values in Decimal Dot System

ElementId	Node1	Node2	Node3	Node1x	Node1y	Node1r	Node2x	Node2y	Node2r	Node3x	Node3y	Node3r
1	1	5	6	61.55970	10.73077	VALUES INSERTED	61.30087	10.71663	VALUES INSERTED	61.12509	10.81949	VALUES INSERTED
2	5	8	6	61.30087	10.71663		61.19482	10.68747		61.12509	10.81949	
3	4	8	5	61.40893	10.63704		61.19482	10.68747		61.30087	10.71663	
4	2	4	5	61.49945	10.72027		61.40893	10.63704		61.30087	10.71663	
5	1	2	5	61.55970	10.73077		61.49945	10.72027		61.30087	10.71663	
6	1	3	2	61.55970	10.73077		61.42972	10.63693		61.49945	10.72027	
7	2	3	4	61.49945	10.72027		61.42972	10.63693		61.40893	10.63704	
8	3	10	4	61.42972	10.63693		61.35214	10.59239		61.40893	10.63704	
9	4	10	8	61.40893	10.63704		61.35214	10.59239		61.19482	10.68747	
10	10	9	8	61.35214	10.59239		61.25537	10.54403		61.19482	10.68747	
11	9	12	8	61.25537	10.54403		61.11742	10.52055		61.19482	10.68747	
12	12	7	8	61.11742	10.52055		61.06530	10.67431		61.19482	10.68747	
13	8	7	6	61.19482	10.68747		61.06530	10.67431		61.12509	10.81949	
14	10	11	9	61.35214	10.59239		61.12890	10.43510		61.25537	10.54403	
15	9	11	12	61.25537	10.54403		61.12890	10.43510		61.11742	10.52055	
16	11	7	12	61.12890	10.43510		61.06530	10.67431		61.11742	10.52055	

* The Variable, Rainfall Values, (monthly and seasonal decacal averages of rainfall) are inserted in columns of Node1r, Node2r and Node3r.

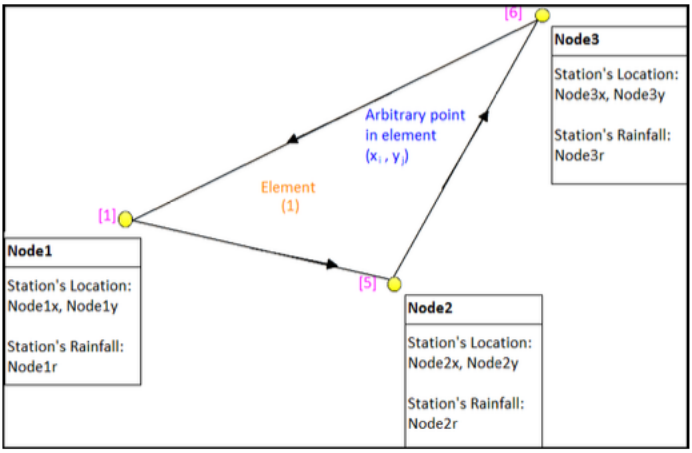

Figure 6: Triangular Element in the Grid and its Associated Values

Where

$$
\begin{aligned}
a_i &= (Node\ 2x \times Node\ 3y) - (Node\ 3x \times Node\ 2y) \\
b_i &= (Node\ 2y - Node\ 3y) \\
c_i &= (Node\ 3x - Node\ 2x) \\
a_j &= (Node\ 3x \times Node\ 1y) - (Node\ 1x \times Node\ 3y) \\
b_j &= (Node\ 3y - Node\ 1y) \\
c_j &= (Node\ 1x - Node\ 3x) \\
a_k &= (Node\ 1x \times Node\ 2y) - (Node\ 2x \times Node\ 1y) \\
b_k &= (Node\ 1y - Node\ 2y) \\
c_k &= (Node\ 2x - Node\ 1x)
\end{aligned}
\tag{4}
$$

and

$$A_n = [a_i + a_j + a_k]/2 \tag{5}$$

aj, bj, cj and ak, bk, ck are cyclic permutations of ai, bi, ci (permuting of Node 1, Node 2 and Node 3 in ai, bi, ci).

A_n values gives the total area of each triangular element in the mesh.

Equations (3), (4) and (5) are the results of solving simultaneously the system of three equations (2) at the corner node points of the triangular element. The system of equations

(6) below has three unknowns $n\alpha 1$, $n\alpha 2$ and $n\alpha 3$ which are related to the known three variables, the x co-ordinate of the stations; Node 1x to Node 3x, the y co-ordinate of the stations; Node 1y to Node 3y and the rainfall values of the stations; Node 1r to Node 3r.

$$\begin{aligned} Node\ 1r &= {}_n\alpha_1 + ({}_n\alpha_2 \times\ Node\ 1x) + ({}_n\alpha_3 \times\ Node\ 1y) \\ Node\ 2r &= {}_n\alpha_1 + ({}_n\alpha_2 \times\ Node\ 2x) + ({}_n\alpha_3 \times\ Node\ 2y) \\ Node\ 3r &= {}_n\alpha_1 + ({}_n\alpha_2 \times\ Node\ 3x) + ({}_n\alpha_3 \times\ Node\ 3y) \end{aligned} \quad (6)$$

Any arbitrary point (xi, yj) of a sub-area of the elemental meshing, the differential volume of rainfall is given by equation (7).

$$dQ = H(x_i, y_j)\ dA \quad (7)$$

Thus the total volume of rainfall for that sub-area, using equation (2), is:

$$Q_n = \iint [\, {}_n\alpha_1 +\ {}_n\alpha_2 x_i +\ {}_n\alpha_3 y_i] dx_i dy_j \quad (8)$$

$$Q_n = A_n[\, {}_n\alpha_1 + \frac{{}_n\alpha_2(Node1x+Node2x+Node3x)}{3} + \frac{{}_n\alpha_3(Node1y+Node2y+Node3y)}{3} \quad (9)$$

The Mean Areal Precipitation of each element is given by Equation (10).

$$H_n = Q_n/A_n \quad (10)$$

The Mean Areal Precipitation of the entire domain is therefore given by Equation (11).

$$\hat{H} = \sum_{n=1}^{16} H_n \quad (11)$$

$$\hat{H} = Q/A \quad (12)$$

Where $Q = \sum_{n=1}^{16} Q_n$ and A= $\sum_{n=1}^{16} A_n$

Tables 3 and 4 give the elemental areas for both the grid and the altered grid. The areas of the elements of the adjusted grid, ranged from approximately 73 to 176 square km. This is an estimated 67 square km less than the elemental areal range of the first grid.

For the Depth-Area Duration Curves, the areas of the elements and accumulatively, the area of the mesh are required. To generate these curves, the H_n values; that is the elements' Mean Areal Precipitation, are ranked in order of highest to lowest areal rainfall values. The corresponding A_n and Q_n values of H_n are ranked accordingly. Thereafter, the Accumulative A_n and the Accumulative Q_n are calculated. Maximum Depth for each of the sub-areas in the ranked order are then determined by dividing the Element Id's corresponding cumulative Q_n value by its Accumulative A_n value. The Area-Depth Duration plots are given by plotting the Accumulative A_n against the Max Depth; that is the Average Precipitation Depth (mm) vs. Area (km^2)

RESULTS AND DISCUSSION

The analysis of the raw data is done under three categories; seasonal, spatial and temporal analysis. For each station, the mean decadal precipitation values for the dry (January to May) and wet (June to December) seasons are represented in Fig. 7. We observe that the maximum rainfall values for both the wet and dry seasons came from Hollis Reservoir station. The largest average decadal rainfall values for the stations were over 500 mm and 1500 mm for the dry and wet seasons respectively. The stations which saw a rainfall reading exceeding the 500 mm marker for the dry season were also surpassing the marker of 1500 mm for the wet season The top four stations with the highest rainfall were the same for both wet and dry seasons; these are Hollis Reservoir, Grosvenor Estate, Newlands Estate and Matura Police Station. This is true for the stations with the lowest average decadal rainfall values as well. These point data locations are Moka Telemet, U.W.I, U.W.I Field Station and River Estate PG. Two of the top four stations with the highest rainfall values, Grosvenor Estate and Hollis Reservoir, corresponded with the top four stations with the highest elevation as seen in Table 5. Also, River Estate PG, UWI and UWI Field Station, the stations with the lowest decadal averages as seen in Fig. 7, corresponded with three of the stations with the lowest elevation.

For each of the months, the average of the mean 10 year rainfall values for all the stations was calculated. This is plotted in Fig. 8. Also, the averages of all the stations' decadal rainfall averages were calculated for each month. The maximum and minimum stations which produced the highest and lowest average 10 year rainfall values respectively, were determined. These two stations are Hollis and UWI whose total decadal average rainfall values are 2921.13 mm and 1531.10 mm respectively.

From the average of all stations mean decadal rainfall, November is the month of most rainfall and March is month of least precipitation; this holds true for the maximum station of Hollis as well. However, for the minimum station, U.W.I, the month of the most precipitation is in August. Though there are these differences among the stations, there is a clear demarcation of the two seasons for all stations with the dry season having the ranks of 8 to 12. Also, it is noticeable that there is a dip in rainfall in the month of September in the rainy season. This occurs after an increase in the rainfall values from the start of the rainy season in June. It is evident, that there is a sharp rise in rainfall for all stations from May to June; this is the intermediate monthly duration between the dry and wet seasons. Similarly, there is a decrease in rainfall values from November to December; December being the last month of the rainy season before the start of the dry season. This month of December can be seen as the transitioning month from wet to dry season as the rainfall values drop consistently thereafter to its lowest in March before its increase and the commencing of the rainy season.

Table 6 shows the Average Areal Precipitation for the meshed domain. The $\bar{H}$ values give the decadal average (2006-2015) areal rainfall for January to December. This is represented in Fig. 9. From the results obtained, in the month of November, the areal precipitation for the grid was the highest. Approximately there were 302.16 mm of rainfall for November. The average areal precipitation of the grid is relatively close to the mean decadal precipitation value of 282.11 mm for all the stations as seen in Fig. 8. Similarly, the month in which there was the lowest precipitation is March for both the average decadal rainfall for all stations and the average areal precipitation for the grid. This decadal mean areal precipitation value from Fig. 8 is 68.24 mm whilst the areal precipitation of the triangulated grid for the period 2006-2015 is approximately, 77.93 mm. Also, we observe from Fig. 9, the dip in rainfall in the month of September. This is a characteristic of Trinidad's rainfall called the "Petit Careme" in which there is a dry spell of 2 to 3 weeks in the middle of September or October (WRA, 2001).

Table 3: Co-ordinates of the Stations and Areas of the Elements for DAD Curve Analysis

NodeId	x Co-ordinate (km)	y Co-ordinate (km)	ElementId	Area of Elements (km^2)
1	657.500	86.580	1	176.30200
2	664.096	85.450	2	97.02970
3	671.770	76.270	3	70.12180
4	674.045	76.293	4	98.02070
5	685.820	85.160	5	11.31760
6	704.980	96.650	6	25.93980
7	711.620	80.630	7	10.53050
8	697.440	82.000	8	5.65234
9	690.905	66.095	9	75.19380
10	680.285	71.387	10	101.74700
11	704.820	54.125	11	128.40300
12	706.020	63.585	12	124.68500
			13	109.03300
			14	26.74160
			15	72.99990
			16	16.26100

Table 4: Bodes of the elements and elements areas in square km for the adjusted grid

NodeId	Stations	ElementId	Node1	Node2	Node3	Elemental Areas
1	River Estate PG	1	1	3	4	176.3020
2	UWI Field Station	2	1	2	3	135.8580
3	Asa Wright Nature Centre	3	2	5	3	73.8499
4	Matelot Rest House	4	3	5	4	97.0297
5	Hollis Reservoir (Quare)	5	5	6	4	109.0330
6	Matura Police Station	6	2	7	5	87.0688
7	Piarco	7	7	8	5	101.7470
8	Arena Dam Pot Gauge	8	8	9	5	128.4030
9	Grosvenor Estate	9	9	6	5	124.6850
10	Newlands Estate	10	8	10	9	72.9999

Table 5: Elevation of the rain Gauge Stations

NodeId	Stations	Elevation AMSL (m)
5	Asa Wright Nature Centre	410
8	Hollis Reservoir (Quare)	203
12	Grosvenor Estate	147
2	Moka Telemet	102
6	Matelot Rest House	67
7	Matura Police Station	54
11	Newlands Estate	43
9	Arena Dam Pot Gauge	36
1	River Estate P.G.	35
4	U.W.I.	27
3	UWI Field Station	7
10	Piarco	5

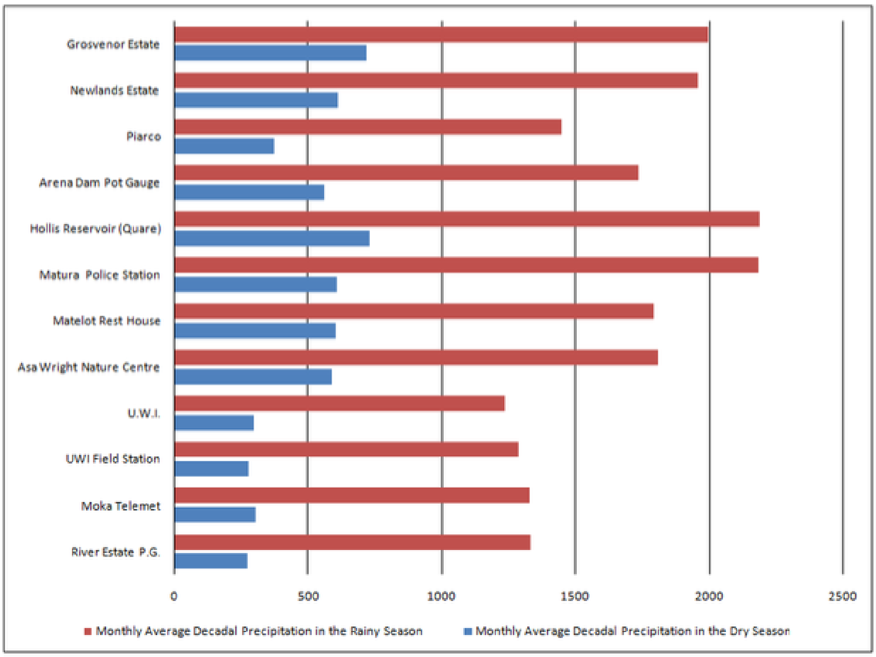

Figure 7: Bar Chart showing Monthly Decadal Rainfall Averages of the Rain Gauge Stations for the Two Seasons

The average areal precipitation of each month for all of the elements in the grid is given by Table 7. For all the elements, the average monthly precipitation during the dry and rainy seasons were plotted in Fig. 10 and 11 below. From the results, generally we observe that elements 4 to 8 have the lowest $\overline{H_n}$ values and elements 1 to 3 and elements 11 to 13 have the largest $\overline{H_n}$ values. From Fig. 4, we observe that elements 1, 2, 3 and 13 are elements which are located in the mountainous regions of the grid with element 1 being the largest element in this domain. Element 11, on the other hand, is located on less mountainous regions of the grid, however, as seen in Table 3, it is the second largest element of the domain. Also, elements 5 to 8, which have low values of $\overline{H_n}$, correspond to the smallest elemental areas in the grid which range from approximately 5.7 to 25.9 square kilometres. Hence we see that the size of the elements and the altitude of the areas are contributory factors in the variation of the areal precipitation throughout the domain. This result obtained of areas of maximum and minimum precipitation is consistent with the factors established which influence Trinidad's rainfall. These factors, according to WRA (2001), are the moisture of the North East Trade Winds and the topography of the island. Thus, we have a decrease in rainfall from the Windward to the Leeward coasts and an increase in rainfall when there is an increase in elevation (WRA, 2001).

The elements of the grid were labelled as small and large. The small elements consisted of elements 8, 7, 5, 16, 6 and 14 and their areas ranged from 5.65234 to 26.74160 square km. Elements 3, 15, 9, 2, 4, 10, 13, 12, 11 and 1 were listed as the large elements of areas 70.12180 to 176.30200 square km. The elements were listed as high and low elevation elements as well. Elements 1, 2, 3, 4, 5, 6, 7 and 13 are high elevation elements whilst elements 8, 9, 10, 11, 12, 14, 15 and 16 are low elevation elements. The high elevation elements were then subdivided into small and large elements. The large high elevation elements are elements 1, 2, 3, 4 and 13 whilst the small high elevation elements are 5, 6 and 7. Also, the large low elevation elements are 9, 10, 11, 12 and 15 and the small low elevation elements are 8, 14 and 16.

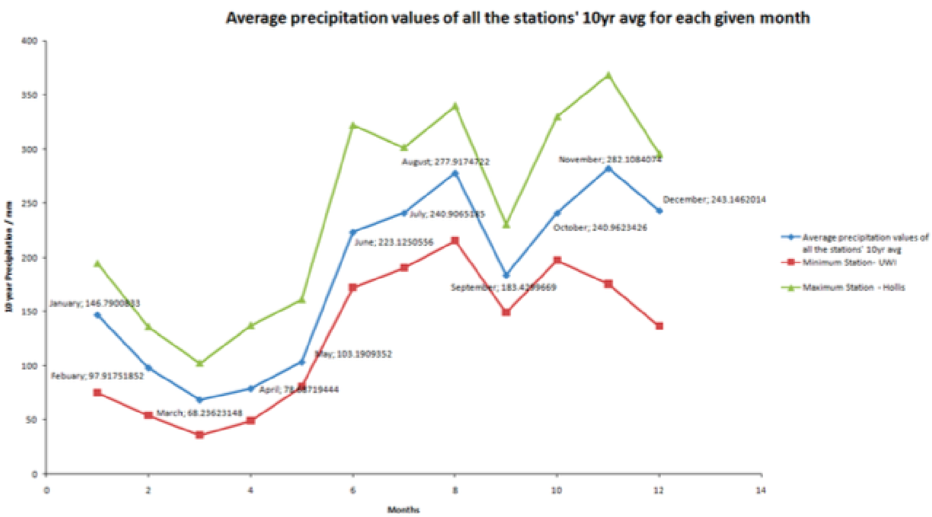

Figure 8: Line Graph showing the Averages of the Monthly Mean Decadal Rainfall Values for all the Rain Gauge Stations

We consider the areal precipitation of the large, small, low and high elevation elements individually. These results are illustrated in Figs. 12 to 19. From Figs. 12 and 13, we observe that from September there are the most deviations of elemental areal precipitation values. The approximate maximum differences are 207 and 232 mm for the large and small elements respectively in the month of November. From Figs. 14 and 15, the differences in the elemental maximum rainfall based on its altitude is less than the differences observed from the elemental sizes. This is consistent with the theory which attributes the size and shape of the element as an indicator of the accuracy of the finite element solution.

The maximum differences in precipitation for the low elevation elements is 216 mm whilst the high elevation elements differ by a maximum 195 mm of rainfall. However, the total differences amongst the minimum to maximum low elevation elements and the minimum to maximum high elevation elements, for all of the months, are approximately the same precipitation value of 1200 mm. Element 8 shows a significant monthly rainfall variation when compared to the other elements of the low elevation plot. This is a direct result of the size of the element; this is a considerably smaller element than any of the other low elevated elements. Neglecting this element, low elevated elements have less elemental rainfall differences. Also, the low elevated elements maintain the same peak months which provides a distinctive rainfall pattern; this is not noted in the high elevated elements during the peak months of the rainy season.

From Fig. 18, it is evident that the areal precipitation for the small high elevation elements display a similar rainfall pattern. Comparing with Fig. 16, the small high elevation elements have less elemental areal precipitation variations than the small low elevation elements. However, these elements vary from the other elements in the grid in terms of their minimum and maximum months. Fig. 17, the areal precipitation for the large low elevation elements, shows more distinctive increasing and decreasing trends than the areal precipitation for the areal precipitation of the large high elevation elements as seen in Fig. 19. Thus, we can derive that for the smaller elements, there are more variations in the finite element solutions than the larger elements and for the low elevation elements, there are more consistency in the estimated solutions when compared to the high elevation elements. As such, the smaller irregularly shaped triangular elements which are located in the mountainous regions of the domain, have the most differences in their monthly areal precipitation when compared to the remaining grid elements; this is as expected.

Table 6: $\overline{H}$ values for Daily and Monthly Analysis of decadal period 2006-2015

Month	$\bar{H}$/ mm
January	163.63192420
February	111.17578350
March	077.93382854
April	089.74206250
May	118.65721760
June	244.90878980
July	258.69023350
August	291.14254860
September	189.29119850
October	260.60139600
November	302.15819580
December	260.94991580

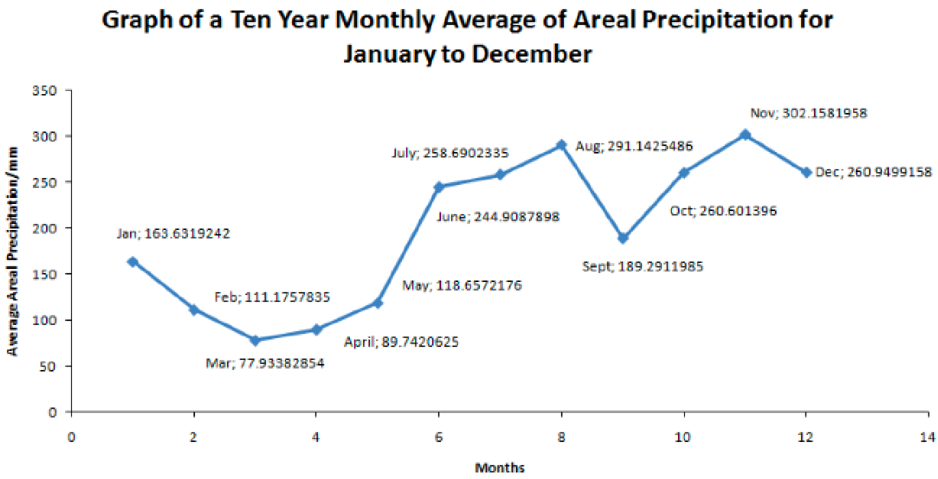

Figure 9: The Average Decadal Areal Precipitation, $\overline{H}_n$

Tables 8 and 9 give the average areal precipitation for the adjusted grid and the average areal precipitation for the elements in the grid respectively. The grid's areal precipitation is represented in Fig. 20. Comparing the results of Fig. 20 with Fig. 9, we observe that both grids have the same rainfall pattern. The annual areal precipitation for the grid of Fig. 4 is 2368.88309434 mm whilst for the altered grid of Fig. 5, there was an annual rainfall value of 2382.78427327 mm. The adjusted grid has an annual rainfall amount of 14 mm more our initial grid. This is despite the area of the adjusted grid being approximately 43 square km less than the initial grid. This indicates that the irregular triangles may have overestimated the areal precipitation over their relatively small areas. An ideal grid is one in which there is a fine mesh of equilateral triangles so that the areal precipitation over the various parts of the domain gives the best approximation of its true or actual areal precipitation.

Table 7: The Average Areal Precipitation, $\bar{H}_n$, of each month, for each of the elements in the domain

ElementID	Jan $\bar{H}_n$	Feb $\bar{H}_n$	Mar $\bar{H}_n$	Apr $\bar{H}_n$	May $\bar{H}_n$	June $\bar{H}_n$
1	148.35666670	099.09000000	069.40000000	072.56333333	098.33333333	199.4333333
2	185.01300000	128.05500000	093.97333333	099.74733333	134.5176667	259.5566667
3	153.73966670	099.81500000	075.93666667	086.97066667	121.4676667	243.3866667
4	131.04333330	073.04666667	057.27666667	057.49666667	076.08666667	163.9896296
5	134.18000000	071.54666667	054.83000000	059.76333333	066.80000000	153.8096296
6	096.92000000	053.18333333	036.77666667	048.18666667	048.09333333	131.2029630
7	093.78333333	054.68333333	039.22333333	045.92000000	057.38000000	141.3829630
8	086.37000000	059.08000000	040.03000000	046.30666667	082.78000000	185.4100000
9	124.63633330	086.36833333	062.36000000	078.74400000	114.28433330	236.9666667
10	152.96077780	109.60944440	073.07333333	091.04511111	128.78322220	265.1462963
11	189.59811110	139.57777780	090.45200000	106.04877780	145.23855560	276.9942963
12	202.14922220	133.38629630	094.26792593	115.11025930	140.82300000	303.5891111
13	187.10188890	126.56462960	090.65259259	112.51992590	130.50100000	293.3377778
14	142.87111110	104.51044440	070.05366667	081.15518519	116.22740740	248.0948148
15	179.50844440	134.47877780	087.43233333	096.15885185	132.68274070	259.9428148
16	192.05955560	128.28729630	091.24825926	105.22033330	128.26718520	286.5376296

ElementID	July H_n	Aug H_n	Sept H_n	Oct H_n	Nov H_n	Dec H_n
1	252.7566667	287.7933333	188.9500000	224.1285185	243.0411111	249.3029630
2	284.7743333	314.3440000	198.9080000	280.9805185	298.4874444	293.5619630
3	253.0676667	297.7506667	194.7146667	267.6005185	255.2507778	233.0119630
4	198.1433333	269.7088889	198.3016667	226.1418519	184.5759259	216.5546296
5	203.3033333	284.7355556	215.5650000	213.5585185	193.5025926	225.3446296
6	180.9600000	254.1922222	203.0550000	185.5066667	179.8248148	181.4450000
7	175.8000000	239.1655556	185.7916667	198.0900000	170.8981481	172.6550000
8	208.4866667	241.8133333	159.5666667	194.3533333	186.6866667	147.1566667
9	242.4576667	273.3206667	180.8046667	240.6120000	249.4096667	200.7423333
10	262.0776667	290.6673333	182.7999048	254.3153333	311.8930000	223.3290000
11	272.8853333	300.7976667	187.4485714	286.1090000	371.4790000	277.8896667
12	290.5082963	306.1813704	199.2059259	311.5938148	391.3493704	321.0289259
13	296.4672963	296.4610370	194.1672593	294.1068148	365.5133704	315.9249259
14	244.5611111	278.5296296	159.7722751	230.037037	323.1450000	229.5979167
15	255.3687778	288.6599630	164.4209418	261.8307037	382.7310000	284.1585833
16	272.9917407	294.0436667	176.1782963	287.3155185	402.6013704	327.2978426

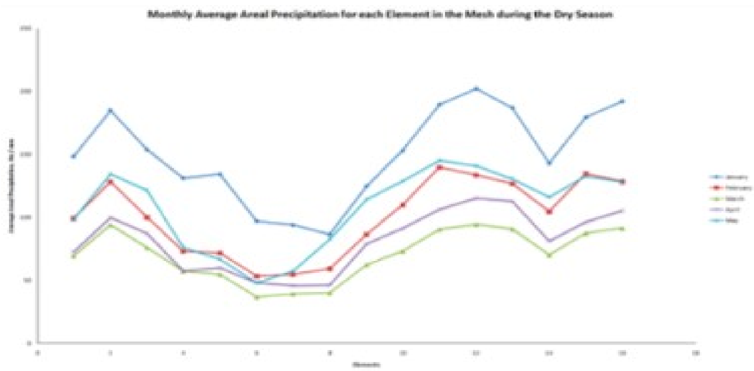

Figure 10: Monthly average areal precipitation of all the elements in the grid for the dry season, January to May

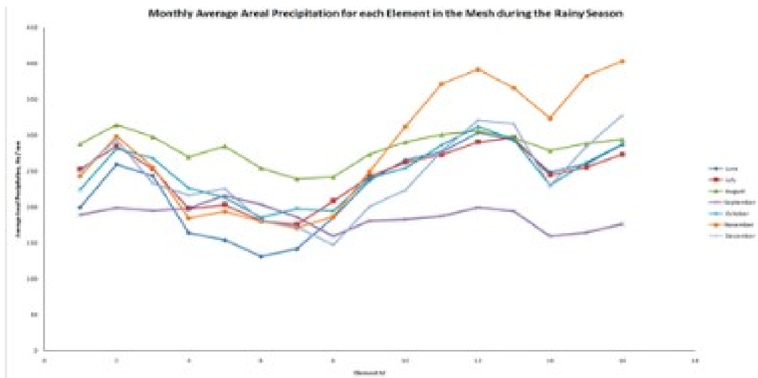

Figure 11: Monthly average areal precipitation of all the elements in the grid for the rainy season, June to December

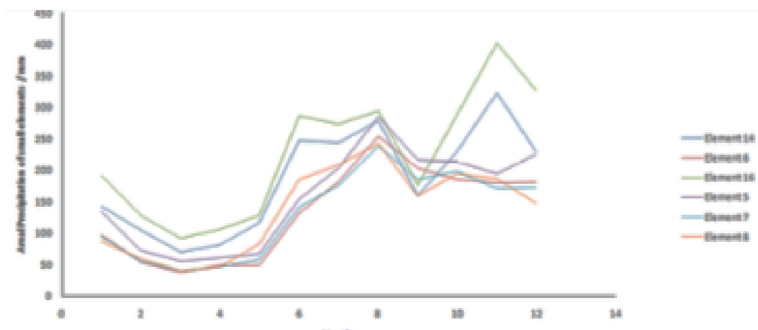

Figure 12: Plot showing the areal precipitation of the small elements for the decadal period

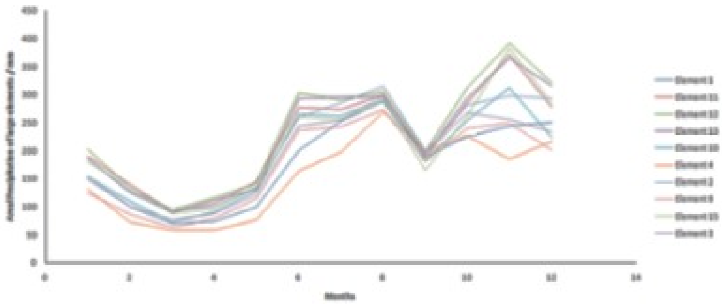

Figure 13: Plot showing the areal precipitation of the large elements for the decadal period

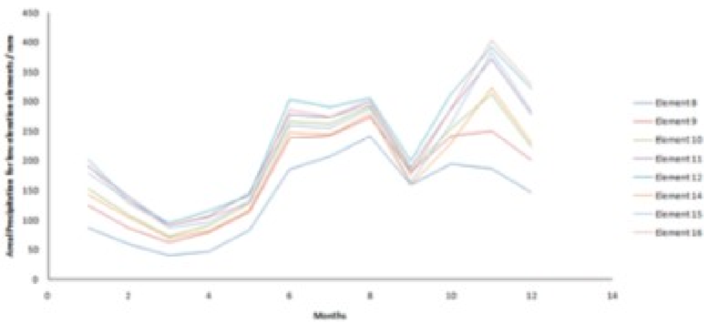

Figure 14: Plot showing the areal precipitation of the low elements for the decadal period

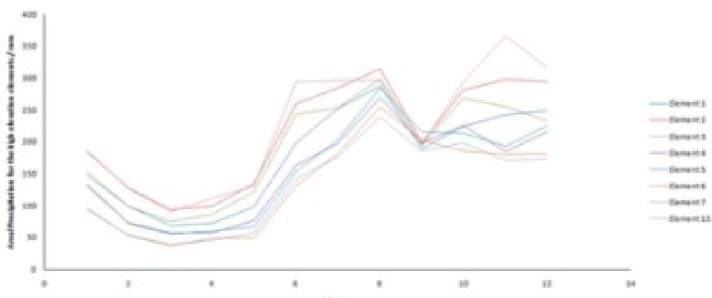

Figure 15: Plot showing the areal precipitation of the high elevation elements for the decadal period

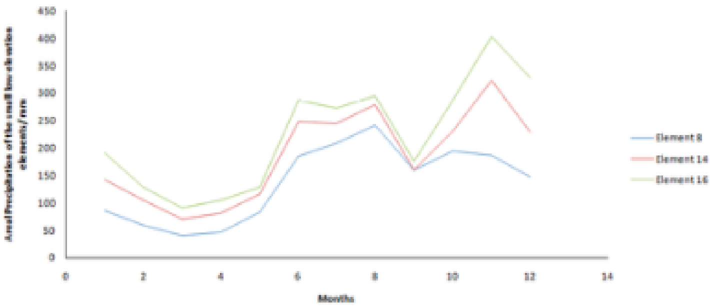

Figure 16: Areal precipitation of the small low elevation elements for the decadal period

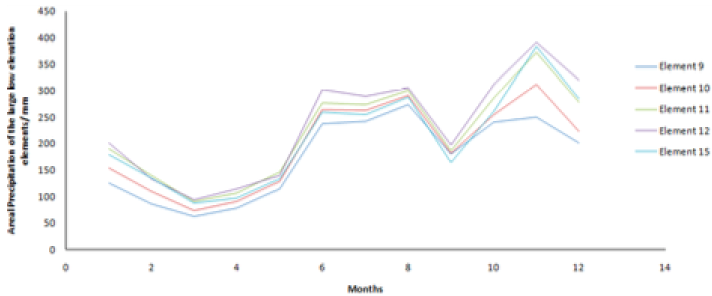

Figure 17: Areal precipitation of the large low elevation elements for the decadal period

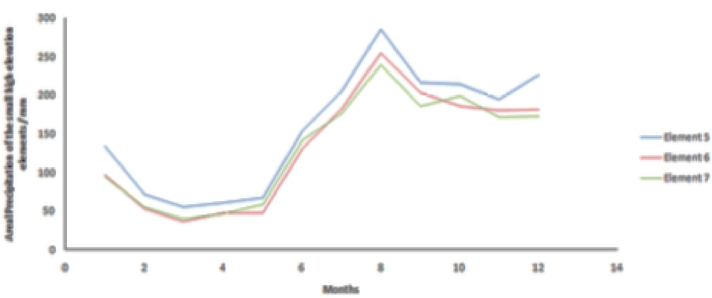

Figure 18: Areal precipitation of the small high elevation elements for the decadal period

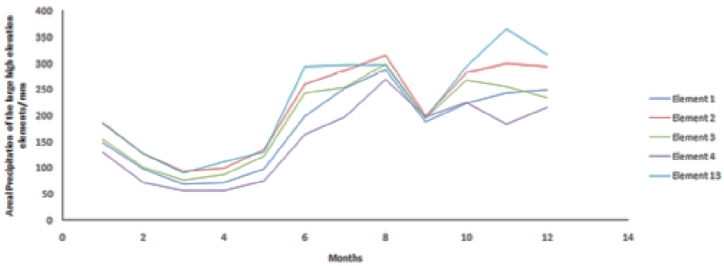

Figure 19: Areal precipitation of the large high elevation elements for the decadal period

Table 8: $\bar{H}$ values for monthly analysis of decadal period 2006-2015 for the adjusted grid

Month	$\bar{H}$ / mm
January	163.7707719
February	111.8236677
March	78.03149356
April	89.89227351
May	119.9260234
June	248.1817711
July	263.6643719
August	295.0659009
September	189.9697803
October	260.3307388
November	303.5589186
December	258.5685616

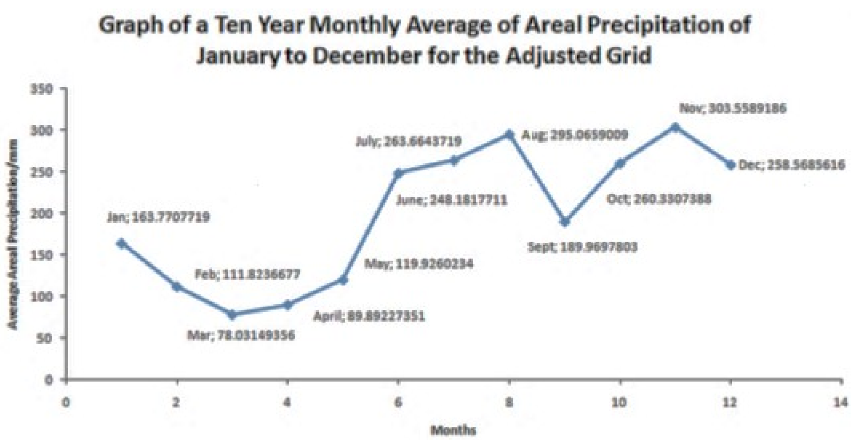

Figure 20: The average monthly areal precipitation for the adjusted grid using decadal averages

According to Chae and Bathe (1989), equilateral triangles give the best triangulated meshing results. These elements are not only non-equilateral triangles but they also have significant size variations from the other triangles in the mesh. Diaz et al. (1983), stated that to improve the finite element solution for the mesh, the initial solution needs to be examined and regions of poor estimation in the domain needs to be identified. According to Diaz et al. (1983), optimization techniques include the adding of new degrees of freedom by the h-method which entails the subdivision of elements. This is done till the error indicators are the constant for all the elements. These estimators are related to the size of the elements. Changing the mesh to obtain a enriched one includes optimizing the configuration of the nodes and redistributing the nodes. Since our elements in the initial the grid have non-equilateral triangles which spans a significant length of the grid but have small areas, adjustments made to the nodal connectivity in our second grid yields more accurate elemental solutions.

From Fig. 21, it is evident that for the adjusted grid, each element displayed more similarity in terms rainfall patterns for all of the months in both the dry and rainy seasons when compared to the initial grid. This is especially noticeable in the dry season where each element maintains a peak or a trough for all of the monthly plots. To a lesser extent, this is also observed in the rainy season with the exception of the months of August and September. These months, although they did not conform to the rainfall pattern of the other months of the grid, the variations in rainfall of respective elements of August and September are comparable.

Table 9: The Average Areal Precipitation,$\bar{H}_n$, of each month, for each of the elements in the adjusted domain

ElementID	JanH_n	Feb H_n	MarH_n	AprH_n	May H_n	June H_n
1	148.3566667	99.0900000	69.4000000	72.56333333	98.33333333	199.4333333
2	118.6100000	71.02666667	51.1600000	56.80000000	80.67666667	181.6500000
3	155.2663333	99.99166667	75.73333333	83.98400000	116.86100000	241.7733333
4	185.0130000	128.0550000	93.97333333	99.74733333	134.5176667	259.5566667
5	187.1018889	126.5646296	90.65259259	112.5199259	130.5010000	293.3377778
6	126.1630000	86.5450000	62.15666667	75.75733333	109.6776667	235.3533333
7	152.9607778	109.6094444	73.07333333	91.04511111	128.7832222	265.1462963
8	189.5981111	139.5777778	90.4520000	106.0487778	145.2385556	276.9942963
9	202.1492222	133.3862963	94.26792593	115.1102593	140.8230000	303.5891111
10	179.5084444	134.4787778	87.43233333	96.15885185	132.6827407	259.9428148

ElementID	July $\bar{H}_n$	Aug $\bar{H}_n$	Sept $\bar{H}_n$	Oct $\bar{H}_n$	Nov $\bar{H}_n$	Dec $\bar{H}_n$
1	252.7566667	287.7933333	188.9500000	224.1285185	243.0411111	249.3029630
2	224.2566667	281.2700000	190.7400000	208.7585185	201.4544444	188.2162963
3	256.2743333	307.8206667	200.6980000	265.6105185	256.9007778	232.4752963
4	284.7743333	314.344000	198.9080000	280.9805185	298.4874444	293.561963
5	296.4672963	296.461037	194.1672593	294.1068148	365.5133704	315.9249259
6	245.6643333	283.3906667	186.7880000	238.6220000	251.0596667	200.2056667
7	262.0776667	290.6673333	182.7999048	254.3153333	311.8930000	223.3290000
8	272.8853333	300.7976667	187.4485714	286.1090000	371.4790000	277.8896667
9	290.5082963	306.1813704	199.2059259	311.5938148	391.3493704	321.0289259
10	255.3687778	288.6599630	164.4209418	261.830703	382.7310000	284.1585833

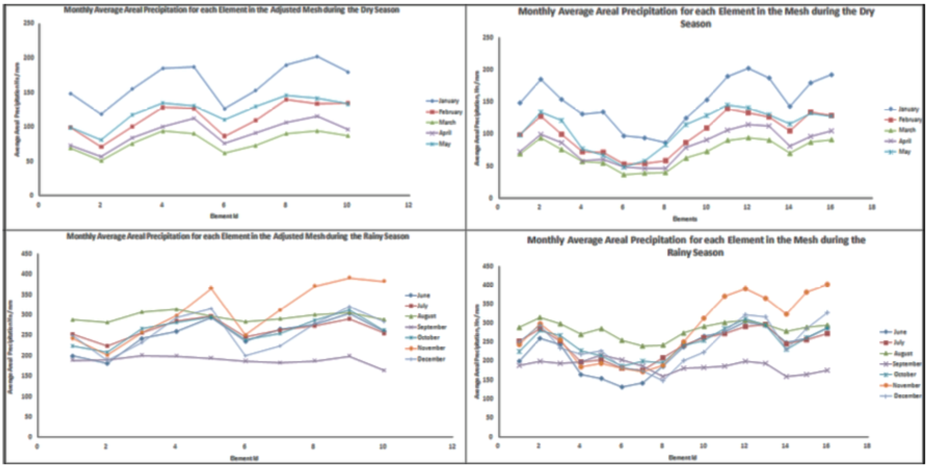

Figure 21: A comparison of the monthly areal precipitation of the elements of the grid and the adjusted grid for both seasons

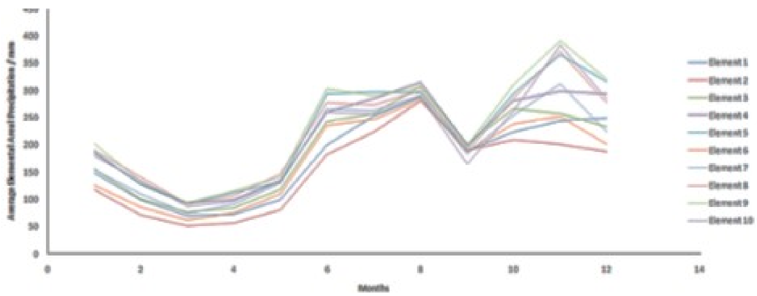

Figure 22: Average areal precipitation for the elements adjusted grid in the various months

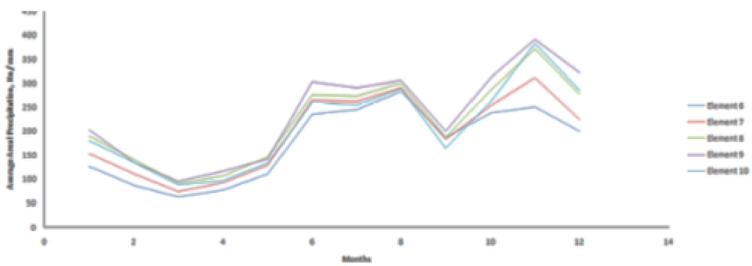

Figure 23: Average areal precipitation for low elevation elements of the adjusted grid

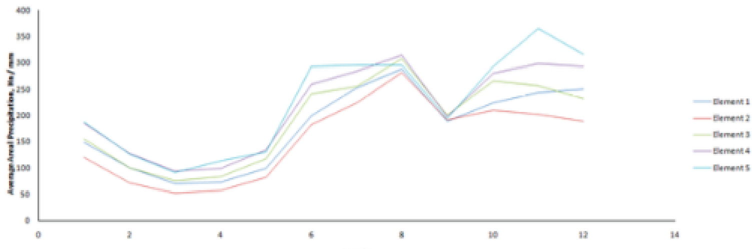

Figure 24: Average areal precipitation for high elevation elements of the adjusted grid

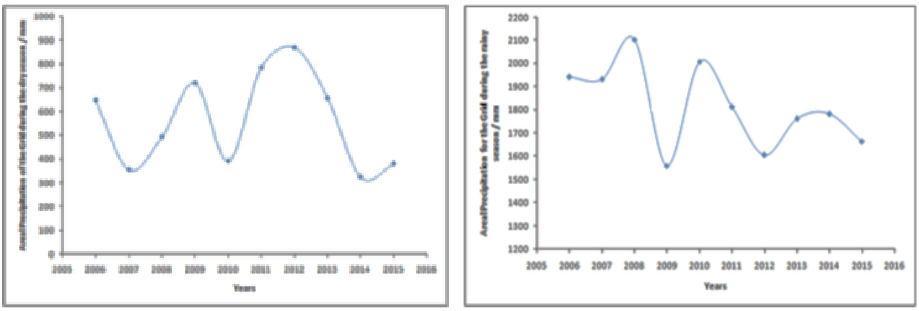

(a) Areal Precipitation for the grid for the dry season

(b) Areal Precipitation for the grid for the rainy season

Figure 25: Areal seasonal precipitation of the grid

For the adjusted grid, there is no longer a classification of the sub-areas in terms of small and large elements; all of the small elements were removed. Hence, we have the rainfall pattern in the various months of the adjusted grid as seen in Fig. 22, is similar to the rainfall patterns of the large elements in the initial grid, Fig. 13. However, for the adjusted grid there is less elemental deviations in rainfall values for the various months. A noticeable change came from Element 4 in the initial grid. After modifying the grid, element 4 of the first mesh was contained in element 2 of the altered mesh. We observe from Fig. 13, that the precipitation plot for element 4 had the most rainfall variations from the other elements particularly from months 6 and 7 as well as months 11 and 12. Our second grid removes this discrepancy.

We observe that as in the case of our initial grid, there are more elemental rainfall differences in the rainy season than the dry season. From Fig. 23, the maximum difference came in November in which there was a difference of approximately 140 mm of rainfall. Similarly, November had the greatest elemental rainfall difference as seen in Fig. 24; its value was 164 mm.

Fig. 25 shows the areal precipitation for the grid within the period 2006 to 2015 for the dry and rainy seasons respectively. From the results, we see that the areal precipitation for the grid in both the dry and rainy seasons are oscillatory in nature with increasing and decreasing areal rainfall for the grid in the various years. However, from Fig. 3.13, we see that the areal precipitation in the dry season oscillates about an average of 560 mm of rainfall whilst for the rainy season, from Fig. 3.14, there is a decrease in the peak rainfall values as the years progressed. This indicates that for the rainy season, even though the areal rainfall values are oscillatory, we are getting dryer rainy seasons as the years progresses from 2006 to 2015. However, as noted by Balek (1983), the seasonal fluctuations and patterns in the tropical regions are predictable and regular. They are relatively stable when compared non-tropical areas where there are erratic rainfall patterns. From the results, it is noted as well, that for the years with the maximum areal precipitation in the dry season corresponded with the years with the minimum areal precipitation in the rainy season, 2009 and 2012. Similarly, the peak years of 2010 and 2014 in the rainy season corresponded with trough years in the dry season (excluding 2008).

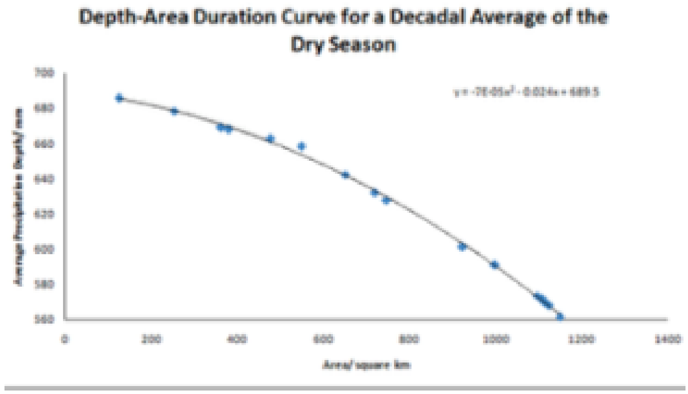

(a) DAD Curve for the dry season

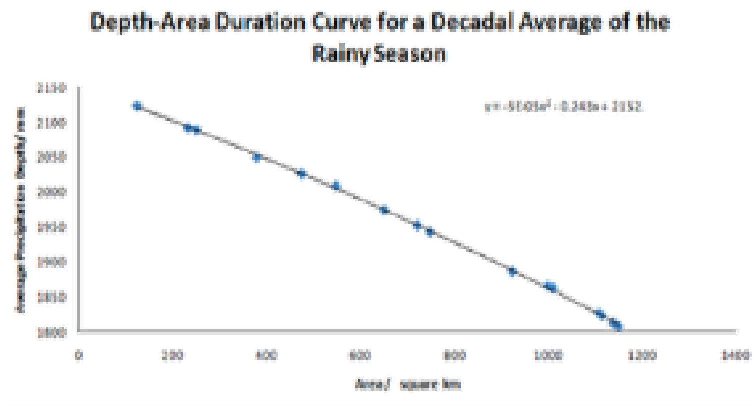

(b) DAD Curve for the rainy season

Figure 26: DAD curves for the grid

DAD Curves display the depth and the area covered by rainfall for a given duration. It gives the spatial variability of rainfall (Balek, 1983). If the rainfall duration is longer, it covers a wider area. This information is crucial for hydrologists and engineers in the design and construction of bridges and drainage systems. DAD curves give the maximum depth of rainfall falling in various areas for different durations. DAD Curves is needed by hydrologists to determine the estimated values of maximum rainfall for each element or area in a given domain or grid; here point rainfall data needs to be converted to aerial precipitation (Mohammadi and Mahdavi, 2009).

Fig. 26 shows the DAD Curves for both the dry and rainy seasons of the grid. As expected we see that as the area increases the average rainfall depth decreases for both seasons. From a study in the Muskingum Basin, Ohio, in which various densities of rain gauges were investigated for a storm. The results showed that the area and density of a network are functions of the standard error of the rainfall averages (Linsley et al. 1975). It was observed that the depth errors of the samples increased when there was an increase in the mean areal precipitation and decreased when the network density, size of domain and duration of rainfall increased (Linsley et al., 1975). Since our DAD Curves were generated for seasons, the average errors of these curves is less than a storm event. We also expect the accuracy of these plots to be greater where there is less rainfall (that is in the plains) and in regions where there are more dense network of rain gauges.

LIMITATIONS OF STUDY AND FUTURE WORK

Mean areal precipitation requires continuous data in which its accuracy is based on the number of observations sites, topographic features of the domain and temporal frequency of precipitation measurements (Teegavarapu, 2022). Thus our model's accuracy is limited by these factors and since the procedure used is dependent on the geometric features, the triangles formed using the position of the gauges (Teegavarapu 2022), the regional parameters such as climate and topography were not fully considered. Future work include incorporating varying precipitation data such as radar data as well as the assessment of results obtained from optimizing the grid.

CONCLUSION

From the Water Resources Agency's Isohyetal Map for Trinidad using rainfall data for Trinidad from 1911 to 1985, it was noted that the North Eastern part of Trinidad has the maximum rainfall with 3800 mm and a minimum contour of 1000 mm which passes through North Western Trinidad. Since these two isohyets have points that are in the grid we expect the average areal precipitation of the grid to be between 1000 and 3800 mm. From the average decadal monthly areal precipitation values obtained, we determine the annual aerial rainfall of the grid to be approximately 2368.8 mm. Thus, it is evident that this method of finite elements in the determination of the areal precipitation of the grid yields consistent results with the areal precipitation of the region given from the isohyetal map. Also, from WRA National Report (2001), the average precipitation over the entire island is 2000 mm. The average areal precipitation of our grid is approximately 400 mm greater than this average. However, this is expected as the North-East Trade Winds brings the greatest rainfall in the North-Eastern highlands of the island which is contained in our mesh.

Declaration of competing interest

The authors declare that they have no known competing financial interests or personal relationships that could have appeared to influence the work reported in this paper.

ACKNOWLEDGEMENTS

Data was obtained from the following sources.

1. Water and Sewerage Authority of Trinidad and Tobago, Water Resources Agency (WRA).
2. The University of the West Indies, St. Augustine Campus, Trinidad and Tobago. Department of Food Production. University Field Station (UFS).
3. Trinidad and Tobago Meteorological Service (MET).

REFERENCES

ATKIN J.E. (1971). Calculation of mean areal depth of precipitation, Journal of Hydrology, Vol. 12, Issue 4, pp. 363-376.

BALEK J. (1983). Hydrology and Water Resources in Tropical Regions. New York: Elsevier.

BALKISSOON S.K. (2014). Rainfall Erosivity and Rainfall Distribution in the Caroni Basin. MPhil's Thesis, University of the West Indies, St Augustine, Trinidad and Tobago.

CHAE S.W., BATHE K.J. (1989). On Automatic Mesh Construction and Mesh Refinement in Finite Element Analysis, Computers and Structures, Vol. 32, Issue 3, pp. 911-936.

DARSAN J. (2013). Beach Morphological Dynamics at Cocos Bay (Manzanilla) Trinidad, Atlantic Geology, Vol. 49, Issue 1, pp. 151-168.

DIAZ A.R., KIKUCHI N., TAYLOR J.E. (1983). A Method of Grid Optimization for Finite Element Methods, Computer Methods in Applied Mechanics and Engineering, Vol. 41, pp. 29-45.

DORF R.C. (2004). The Engineering Handbook Second Edition. CRC Press, pp. 96-98

KANITHI V., KANHAI C. (2006). Landslides in Trinidad - A Geotechnical Study. Fourth LACCEI Interna- tional Latin American and Caribbean Conference for Engineering and Technology.

LINSLEY R.K. Jr., KOHLER M.A., PAULHUS J.L.H. (1975). Hydrology for Engineers, Second Edition. McGraw- Hill.

MAMPITIYA L., RATHNAYAKE N., LEON L.P., MANDALA V., AZAMATHULLA H.M., SHELTON S., HOSHINO Y., RATHNAYAKE U. (2023). Machine Learning Techniques to Predict the Air Quality Using Meteorological Data in Two Urban Areas in Sri Lanka, Environments, Vol. 10, Issue 8.

MOHAMMADI S.E., MAHDAVI M. (2009). Investigation of Depth - Area Duration Curves for Kurdistan Province, World Applied Science Journal, Vol. 6, Issue 12, pp. 1705-1713.

NOAA (National Oceanic and Atmospheric Administration). NWS (National Weather Service) River Forecast Center, Arkansas-Red Basin. Point Precipitation Measurement, Areal Precipitation Esti- mates And Relationships To Hydrologic Modeling. http://www.srh.noaa.gov/abrfc/?n=map.

REDDY J.N. (1993). An Introduction to the Finite Element Second Edition. Mc Graw-Hill International Editions, Engineering Mechanics Series.

SHRIVASTAVA G.S. (2003). Estimation of Sustainable Yield of Some Rivers in Trinidad, Journal of Hydrologic Engineering, Vol. 8, Issue 1, pp. 35-40.

SRIVASTAVA R. Water Resources Engineering, Lecture Notes. Kanpur: Indian Institute of Technology, pp. 1-25.

SYNNATSCHKE S. Secrets of the West. Geographic Tools Co-ordinate Conversion and Datum Transfor- mation; 2002-2017. http://www.synnatschke.de/geo-tools/coordinate-converter.php. Accessed April 15, 2016.

TASK COMMITTEE ON HYDROLOGY. (1996). Handbook of Management Group D of the American Society of Civil Engineers. Hydrology Handbook, Second Edition. American Society of Civil Engineers.

TAYLOR C. Toolbox. Geographic/UTM Co-ordinate Converter. http://home.hiwaay.net/taylorc/toolbox/geography/geoutm.html. Accessed April 12, 2016.

TEEGAVARAPU R.S.V. (2022). Mean areal precipitation estimation: methods and issues. Rainfall, Elsevier, pp. 217-260

The Cropper Foundation. Nc North Caroni Plains Case Study. Trinidad and Tobago: The Cropper Foundation.

U.S. Department of the Interior. U.S. Geological Survey. The USGS Water Science School 2016. http://water.usgs.gov/edu/100yearflood.html. Accessed April 2, 2016.

WASA (Water and Sewerage Authority of Trinidad and Tobago) 2013. Adopt A River TT, Watershed Maps. http://www.adoptarivertt.com. Accessed February 22, 2016.

WASA (Water and Sewage Authority of Trinidad and Tobago). Water Resources Agency (WRA), Water Resources Assessment of Trinidad and Tobago. Trinidad and Tobago: WRA.

WRA (Water Resources Agency) for the Ministry of the Environment. (2001). National Report on Integrating The Management of Watersheds and Coastal Areas in Trinidad and Tobago. Trinidad and Tobago: WRA.